frontiers in Materials

MINI REVIEW
published: 16 April 2021
doi: 10.3389/fmats.2021.628633

Additively Manufactured Absorbable Porous Metal Implants – Processing, Alloying and Corrosion Behavior

Holger Jahr[1,2], Yageng Li[3], Jie Zhou[2], Amir A. Zadpoor[2] and Kai-Uwe Schröder[4]*

[1] Department of Orthopedic Surgery, Maastricht UMC+, Maastricht, Netherlands, [2] Department of Biomechanical Engineering, Delft University of Technology, Delft, Netherlands, [3] Beijing Advanced Innovation Center for Materials Genome Engineering, School of Materials Science and Engineering, University of Science and Technology Beijing, Beijing, China, [4] Institute of Structural Mechanics and Lightweight Design, RWTH Aachen University, Aachen, Germany

Treating large bone defects is still a clinical challenge without perfect solution, mainly due to the unavailability of suitable bone implants. Additively manufactured (AM) absorbable porous metals provide unparalleled opportunities to realize the challenging requirements for bone-mimetic implants. Firstly, multi-scale geometries of such implants can be customized to mimic the micro-architecture and mechanical properties of human bone. The interconnected porous structure additionally increases the surface area to facilitate adhesion and proliferation of bone cells. Finally, their absorption properties are tunable to maintain the structural integrity of the implant throughout the bone healing process, ensuring sufficient loadbearing when needed and full disintegration after their job is done. Such a combination of properties paves the way for complete bone regeneration and remodeling. It is important to thoroughly characterize the biodegradation behavior, mechanical properties, and bone regeneration ability when developing ideal porous absorbable metal implants. We review the state-of-the-art of absorbable porous metals manufactured by selective laser melting (SLM), with a focus on geometrical design, material type, processing, and post-treatment. The impact of the latter aspects on absorption behavior, resulting mechanical properties, and cytocompatibility will also be briefly discussed. In comparison to their solid inert counterparts, AM absorbable porous metals (APMs) have shown many unique properties and hold tremendous potential to further optimize their application-specific performance due to their flexible geometrical design. We further highlight challenges in adopting AM APMs for future Orthopedic solutions.

Keywords: selective laser melting, absorbable implants, structure, corrosion, biomechanics

OPEN ACCESS

Edited by:
Fabio Scenini, The University of Manchester, United Kingdom

Reviewed by:
Sviatlana V. Lamaka, Universidade de Lisboa, Portugal
Endzhe Matykina, Complutense University of Madrid, Spain

****Correspondence:***
Holger Jahr
h.jahr@maastrichtuniversity.nl

Specialty section:
This article was submitted to Environmental Materials, a section of the journal Frontiers in Materials

Received: *12 November 2020*
Accepted: *23 March 2021*
Published: *16 April 2021*

Citation:
Jahr H, Li Y, Zhou J, Zadpoor AA and Schröder K-U (2021) Additively Manufactured Absorbable Porous Metal Implants – Processing, Alloying and Corrosion Behavior. Front. Mater. 8:628633. doi: 10.3389/fmats.2021.628633

INTRODUCTION

Despite their self-healing abilities, large bone defects do not heal spontaneously and globally require millions of bone grafting procedures annually (Wu et al., 2014; Zhang L. et al., 2019). At present, 15–20% of the Western World population is 65 years or older and our aging society will soon face a dramatic increase in the demand for bone implants. This will cause increased

medical care costs as well as patient morbidity and mortality (Geetha et al., 2009; Fayaz et al., 2011; Loi et al., 2016). Current clinically applied bone grafts comprise autografts (a person's own bone tissue), allografts (donor bone), and xenografts (non-human tissue). While devitalized allografts provide osteoconductive scaffolds of compromised mechanical stability for smaller defects (Giedraitis et al., 2014; Allsopp et al., 2016). Allografts and xenografts hold risks such as transplant rejection due to alloimmunity, transmitting diseases, infections, and compromised osteogenesis (Dimitriou et al., 2011). Therefore, autografts are the superior gold standard. However, they suffer from a limited supply, donor site morbidities, and complication rates of up to 40% (Van der Stok et al., 2011; Wang and Yeung, 2017).

Implants to treat critical-sized bone defects are, thus, particularly sought after on a bone grafts and substitutes market being valued at $4.15 billion by 2026 (Zhao et al., 2017; Polaris Market Research, 2020). Apart from being biocompatible, an ideal bone substitute might have a fully interconnected porous structure to allow for bone ingrowth and possess bone-mimetic mechanical properties to provide sufficient support, while avoiding stress shielding (Wen et al., 2001; Oh et al., 2003; Zadpoor, 2015). Highly porous metal implants were, therefore, introduced to improve biomaterial properties of traditional solid metals. With appropriately designed porosities, surface coefficients, and elastic modulus (Young's modulus), they already mimic characteristics of cancellous bone (Amin Yavari et al., 2013; Matassi et al., 2013). Further advantages of 3D-printed biomedical metals over traditional implants include cost-efficiency, personalized design, and implantation site-specific tunable mechanical performance (Yan et al., 2018). However, like traditional solid permanent implants, they are still at risk of implant-associated infections or may require revision surgeries, with potential complications and unnecessary hospitalization and rehabilitation costs (Hexter et al., 2018).

Geometrically ordered AM porous metal implants with proper absorption profiles now offer these unique material properties and the possibility to fully regenerate bony defects with native bone. Absorbable implants would further allow regenerating bone tissue to replace the implant instead of growing around it or just into its interconnected pores. Given the implant's complete disintegration, any risk of long-term infection would disappear with it – as opposed to permanently retained implants (Chen et al., 2014). So far, it has been challenging to produce porous absorbable biomaterials fulfilling all these requirements and the quest for ideal bone substituting materials is still booming (Oryan et al., 2014). We will specifically focus on absorbable porous implants manufactured by SLM technology, as AM biodegradable metals were recently reviewed (Li et al., 2020a), and summarize the impact of topological design- and material type-dependent differences in the corrosion behavior and corresponding mechanical properties. Furthermore, present shortcomings in adopting these implants for orthopedic applications and future opportunities will be briefly discussed.

ADDITIVE MANUFACTURING OF ABSORBABLE METAL IMPLANTS

Additive Manufacturing Technologies

Current bone-substituting porous biomaterials may comprise polymers, ceramics, and metals (Do et al., 2015). Polymer-based biomaterials offer biofunctionalization and tailored biodegradation through design flexibility (Liu and Ma, 2004), while ceramic-based biomaterials are recognized for their favorable biodegradability and superior osteoconductivity (Seitz et al., 2005). For fully load-bearing applications in humans the former are too soft, while the latter are too brittle (Zhang L. et al., 2019). Metallic implants, on the other hand, have remarkable strength and energy absorption capacity, making them most suitable for such applications (Chen and Thouas, 2015). Complex design considerations are required to fabricate ideal porous metal bone implants. There are three main types of metal AM techniques, (i) directed energy deposition (DED), (ii) powder bed fusion (PBF), and (iii) binder jetting, which are described elsewhere in more detail (DebRoy et al., 2018; Li et al., 2020a). Generally, DED and PBF are both direct AM metal printing techniques, which can be further sub-divided by their heat source. Selective laser melting (SLM, **Figure 1**) is a laser-based PBF technology, also known as direct metal laser melting (DMLM) or laser powder bed fusion (LPBF). A more comprehensive overview on AM techniques for bio-inert metals also addresses their limitations (Li et al., 2020a). At present, LPBF is considered the most appropriate method for building complex porous structures and yet only absorbable porous metals meet all requirements to become ideal bone substitutes (Liu et al., 2017; Li et al., 2020a).

In contrast to bio-inert metals, AM absorbable metals (especially Mg and Zn) have low boiling temperatures and high chemical activities, posing new challenges for LPBF processing (Qin et al., 2019). Inappropriate processing conditions may cause defects, such as voids, lack of fusion, rough surfaces, severe residual stresses, and distortions. Even for Fe, evaporation can occur at high laser intensities (Kruth et al., 2004) and precise process control is, therefore, essential to successfully fabricate topologically ordered porous implants from absorbable metals by AM.

The type of PBF process applied potentially differentially affects the mechanical properties of porous metal products. Internal pores, inclusions, and cracks inside the struts of an implant can deteriorate its mechanical properties (Qin et al., 2019; Li et al., 2020a). Manufacturing defects of AM porous Zn may act as crack initiation sites, potentially shortening the fatigue life of an implant (Ahmadi et al., 2018). Optimizing the energy density tends to improve densification, and, thus, mechanical properties of SLM Mg alloys [e.g., AZ91 (Wei et al., 2014)], while different SLM process parameters affect the size and orientation of grains, thereby affecting mechanical properties as well (Manakari et al., 2016; Qin et al., 2020). Absorbable porous metals generally tend to have much finer grain sizes than their conventionally produced counterparts. This can improve

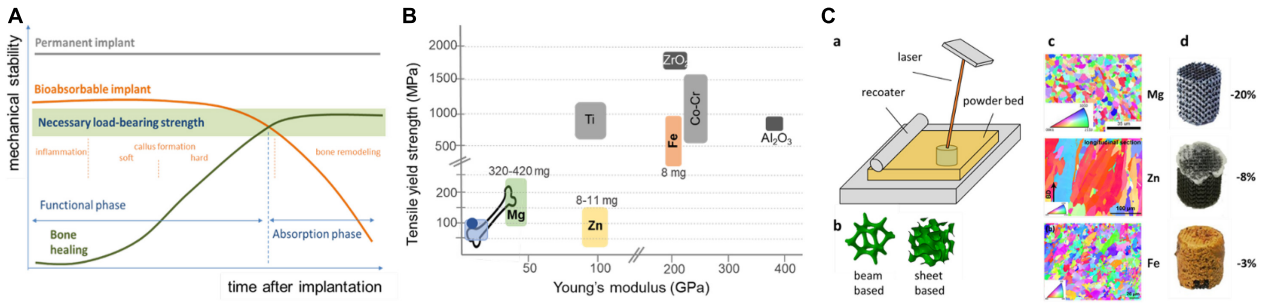

FIGURE 1 | Schematic representation of requirements, material properties, and corrosion characteristics of absorbable metals for bone repair. **(A)** Relationship between corrosion speed-dependent mechanical support (orange line) of an absorbable implant (Hermawan, 2018) and projected mechanical support by bone regeneration (green line). Stages of bone healing are indicated in orange. Dependent on the defect site and size, mechanical implant integrity should remain high enough for about 3–6 months, to ensure initial mechanical support prior to implant failure by progressive corrosion. **(B)** Comparison of mechanical properties of selected biomaterials to those of bone (lower left values = trabecular, upper right values = cortical), polymers [e.g., poly(lactic acid), poly(glycolic acid), or polyhydroxybutyrate in light blue; polyetheretherketone in dark blue], Mg/alloys (green), titanium (Ti)/alloys (gray), Zn/alloys (yellow), iron/steel (brownish), cobalt-chromium (Co-Cr)/alloys (light gray), and ceramics (ZrO_2 and Al_2O_3, dark gray). Age- and gender-dependent Dietary Intake Recommendations (DRI) for Mg, Zn and Fe (in mg) are values for older adults (females-males) (Marian and Sacks, 2009). Note that DRI of Mg is 42 times higher than that of Fe and Zn, respectively. **(C)** Schematic of an SLM process (a) with different topological designs of absorbable metals (b), and Electron Back-Scattered Diffraction (EBSD) images of these SLM metals (c), next to the macroscopic appearance of identically designed scaffolds with their respective weight loss (%) after 28 days of standardized quasi-physiological *in vitro* absorption (d). Note the white and brownish corrosion products on Zn and Fe scaffolds, respectively.

their strengths according to the Hall-Patch relationship (Li et al., 2018a, 2019a, 2020d).

Absorbable Metal Families

Recently, absorbable (ASTM F3160-16), or "*biodegradable*," metals received increasing interest as they possess excellent mechanical properties and degrade in the human body without concerning long-term fatigue damage and revision surgery as compared to permanent counterparts (Do et al., 2015; Liu et al., 2017; Hermawan, 2018). The currently considered absorbable metal families comprise iron (Fe), magnesium (Mg), and zinc (Zn) (Li et al., 2020a; Wang et al., 2020). A comparison of the different mechanical properties of selected biomaterials to those of native bone illustrates the attractiveness of Mg, and its alloys, for load-bearing Orthopedic applications, and why Fe would benefit relatively the most from a decreasing Young's modulus through increasing porosity (**Figure 1B**).

In contrast to traditional permanent implants with almost constant mechanical properties, those of absorbable implants are supposed to change with time. The projected different and increasingly load-bearing phases of bone tissue regeneration have to keep pace with the corrosion speed-dependent decreasing mechanical support by the implant (**Figure 1C**).

Degradation behavior of AM absorbable bulk and porous metals are compared in **Table 1**. Importantly, the influence of loading on their corrosion behavior is currently poorly appreciated. Absorption of AM porous absorbable metals (PAM) can, however, be controlled not only by their material type or chemical composition (i.e., alloying), but also through their microstructure and geometrical design (Li et al., 2020a).

Corrosion Behavior of Absorbable Metals

Depending on their anatomic location, healing rates of bone may differ. Most Orthopedic and cardiovascular applications require mechanical support of at least three and 4 months, respectively, ideally being fully absorbed within 2 years (Zheng et al., 2014; Francis et al., 2015; Venezuela and Dargusch, 2019). Bone fixation devices are further suggested to have degradation rates of less than 0.5 mm/year (Chen et al., 2014; Zheng et al., 2014). In contrast, there is no widely accepted criterion for the corrosion rate of absorbable implants. Controlling degradation speed *in situ* is thus utmost important to avoid premature implant failure and proper corrosion testing of absorbable metallic materials *in vitro* is crucial. Logically, ideal degradation rates would match the location-specific bone regeneration pace (DebRoy et al., 2018). Therefore, means to control the corrosion rates of PAMs are highly sought after. Absorbable metals, and their corrosion products, must further be biocompatible, which will be briefly discussed in section "Biocompatibility and Clinical Application Potential".

The electrode potential values of pure Fe, Mg, and Zn are −0.44, −2.37, and −0.76 V, respectively (Zheng et al., 2014). This suggests the lowest and highest degradation rates for Fe and Mg, respectively, with Zn having an intermediate rate. Biodegradation changes mechanical properties and fatigue behavior of AM PAMs. It decreases the fatigue life of SLM porous Mg and Fe (Christen et al., 2013; Nune et al., 2016): SLM porous absorbable Mg and Fe showed decreasing yield strengths and stiffnesses within 28 days of *in vitro* degradation under quasi-physiological conditions (i.e., in revised simulated body fluid, r-SBF). Currently, uncoated AM porous Mg and its alloys appear to corrode too fast and may prematurely fail *in vivo*.

Solid Zn implants corrode too slowly for most orthopedic applications and first 3D-printed Zn alloys recently improved this (Wen et al., 2018a,b). Surprisingly, after 28 days of biodegradation under the same conditions as for Mg and Fe, SLM porous Zn revealed increased mechanical properties as compared to as-built controls (Li et al., 2018a,b, 2020c),

which was explained by formation of degradation products. Those are 5-times harder than AM Zn itself (Li et al., 2018a) and tightly bind to AM Zn (Li et al., 2020b). Vascular applications of zinc-based alloys were recently critically reviewed (Mostaed et al., 2018).

Alloying-Dependent Corrosion Behavior

During 28 days of *in vitro* corrosion, AM WE43 implants lost almost 20% of their weight, whereas AM Fe and Zn exhibited only 3% and 8% weight loss, respectively (Li et al., 2018b; **Figure 1A**). As Mg generally degrades too fast and Fe too

TABLE 1A | Comparison of mechanical properties of selected solid and porous absorbable metals produced by SLM.

Metal	Alloy	Unit cell design	Porosity (%)	Testing method	Elastic modulus (GPa)	Ultimate strength (MPa)	Yield strength (MPa)	References
Mg	pure			indentation	27–33			Ng et al., 2011a
	pure			indentation	33–35			Ng et al., 2011b
	AZ91D			tensile		296	254	Wei et al., 2014
	WE43			tensile	45.7 ± 1.5	308	296.3 ± 2.5	Zumdick et al., 2019
	Mg			compression			51	Zhou et al., 2016
	Mg-1Zn			tensile			148	Wei et al., 2019
	Mg-2Zn						71	
	Mg-4Zn						60	
	Mg-6Zn						45	
	Mg-8Zn						44	
	Mg-10Zn						63	
	Mg-12Zn						74	
Fe	pure			tensile	215.8 ± 20	411.5 ± 25	305.3 ± 20	Song et al., 2014a
	pure			tensile	208 ± 16	357 ± 22	256 ± 17	Song et al., 2014b
	Pure			compression			200	Montani et al., 2017
Zn	Pure			tensile	14–32	132–138	108–122	Wen et al., 2018b
	pure			tensile	20.47 ± 5.71	137.9 ± 2.48	122.13 ± 2.61	Wen et al., 2018a
	pure			compression			99 ± 22	Montani et al., 2017
	pure			tensile		117–133	93–110	Qin et al., 2020
	pure			compression			146	Shuai et al., 2018c
	Zn			tensile	12.2 ± 2.4	61.3 ± 5.0	43.2 ± 3.1	Yang Y. et al., 2018
	Zn-1Mg			tensile	18.8	126.3 ± 3.6	74.1 ± 3.8	
	Zn-2Mg				25.2	161.8 ± 5.6	117.4 ± 5.4	
	Zn-3Mg				48.2 ± 4.2	222.3 ± 8.2	152.4 ± 4.8	
	Zn-4Mg				57.5 ± 4.8	166.4 ± 7.4	131.6 ± 7.5	
	Zn-2Al					141.7–192.2	121.4–170.5	
porous Mg	WE43	lattice	76.20	compression		15		Kopp et al., 2019
	WE43			bending		20–23		Witte et al., 2016
	WE43	diamond	67	compression	0.77	27	23	Li et al., 2018b
porous Fe	Fe	cubic	66.72 ± 2.3	compression		135 ± 5.2	70.3 ± 4.2	Shuai et al., 2020
	Fe-25Mn	sheet	42	compression		221.7 ± 10.9	137 ± 8.4	
	Fe-35Mn				33.5 ± 1.7	304.0 ± 7.4	89.2 ± 1.9	Carluccio et al., 2020
	Fe	diamond	84.6 ± 0.4	compression	1		11.4	Li et al., 2019a
			69.7 ± 0.2		1.4		29	
			70.3 ± 0.5		1.8		30.7	
			58.9 ± 0.3		2.8		53.6	
	Fe	diamond	73	compression	1.8		23.7	Li et al., 2018a
	Fe + 28d				1.6		22.4	
porous Zn	Zn	diamond	72.6 ± 2.3	compression	399.765		4.165	Li et al., 2020c
		diamond	68.5 ± 2.3		457.085		6.31	
			62.0 ± 2.5		785.67		10.835	

AZ91D (8.3–9.7% Al, ≤0.03% Cu, ≤0.005% Fe, ≤0.002 Ni, 0.35–1.0% Zn, 0.15–0.5% Mn, ≤0.1 Si, 0.02% other metals); WE43 (UNS M18430; rare earths 2.4–4.4%, 3.7–4.2% Y, 0.4% Zr).

TABLE 1B | Corrosion behavior of selected solid and porous absorbable metals produced by SLM.

Material	Alloy composition	Unit cell design	Porosity (%)	Pore size (mm)	Duration (days)	Testing medium	Control	Weight loss (%)	CRI (mm/year)	CRE (mA/cm^2)	References
Mg	Mg				10	SBF		13.30			Zhou et al., 2016
	Mg-1Sn							7.70			
	Mg-3Sn							14.80			
	Mg-5Sn							19.10			
	Mg-7Sn							22.50			
	AZ61				6				1.2–2.7		He et al., 2017
	ZK60				7	SBF			2.1	44.2	Shuai et al., 2018b
	ZK60-0.2Cu								2.4	60.4	
	ZK60-0.4Cu								2.5	85.3	
	ZK60-0.6Cu								17	485.7	
	ZK60-0.8Cu								30	827.5	
	ZK30					SBF				131 ± 14	Shuai et al., 2018a
	ZK30-1Al									68 ± 6	
	ZK30-3Al									24 ± 6	
	ZK30-5Al									156 ± 26	
	ZK30-7Al									340 ± 28	
	Mg-6Zn-0.5Zr				28	SBF			1.58 ± 0.21	36.2 ± 2.3	Yang Y. et al., 2018
Fe	Fe					HANKS				6.2 ± 0.1	Carluccio et al., 2019
	Fe-2Pd-2.5bredigite				21	SBF			0.22	17.78	Gao et al., 2019
	Fe-2Pd-5bredigite				21				0.38	31.62	
	Fe-2Pd-10bredigite				21				0.5	39.81	
	Fe-4Pd-2.5bredigite				21				0.41	34.67	
	Fe-4Pd-5bredigite				21				0.6	50.12	
	Fe-4Pd-10bredigite				21				0.76	63.09	

(Continued)

TABLE 1B | Continued

Material	Alloy composition	Unit cell design	Porosity (%)	Pore size (mm)	Duration (days)	Testing medium	Control	Weight loss (%)	CRI (mm/year)	CRE (mA/cm^2)	References
Zn	Zn				21	HANKS			0.038–0.04	1.6–4.29	Qin et al., 2020
	Zn				21	SBF			0.081	7.76	Shuai et al., 2018c
	Zn-2Ag				21	SBF			0.086	5.01	
	Zn-4Ag				21	SBF			0.107	1.47	
	Zn-6Ag				21	SBF			0.114	9.56	
	Zn-8Ag				21	SBF			0.133	13.94	
	Zn-2Al				14	SBF			0.13–0.16	7.07–11.75	Shuai et al., 2019a
	Zn				28	SBF			0.18 ± 0.03	9.24 ± 1.21	Yang Y. et al., 2018
	Zn-1Mg				28	SBF			0.14 ± 0.01	5.86 ± 1.42	
	Zn-2Mg				28	SBF			0.13 ± 0.03	4.63 ± 0.95	
	Zn-3Mg				28	SBF			0.10 ± 0.02	3.62 ± 0.76	
	Zn-4Mg				28	SBF			0.11 ± 0.04	3.71 ± 0.87	
porous Mg	WE43		76.20	1131	21	DMEM	CO_2	40.20			Kopp et al., 2019
	WE43				3	HANKS	bioreactor	25			Witte et al., 2016
	WE43	diamond	67	600	28	r-SBF	HEPES	20.70	0.23	21–61	Li et al., 2018b
porous Fe	Fe	cubic	66.72		28	SBF		5.3	0.09 ± 0.02	7.38 ± 3.21	Shuai et al., 2020
	Fe-25Mn							13.4	0.23 ± 0.05	51.25 ± 7.52	
	Fe35Mn	sheet	42%	400	28	HANKS	CO_2,dynamic		0.42 ± 0.03	68.5 ± 2.1	Carluccio et al., 2020
	Fe	diamond	84.6	800	28	r-SBF	bioreactor	16.7	0.2		Li et al., 2019a
			69.7					10.3	0.14		
			70.3					8.9	0.17		
			58.9	400				5.1	0.11		
	Fe	diamond	73%		28	r-SBF	HEPES	3.10	0.03	102.8 ± 19.2	Li et al., 2018a
porous Zn	Zn	diamond	72.6	700	28	r-SBF	bioreactor	11.9	0.17		Li et al., 2020c
			68.5	graded			HEPES	7.9	0.14		
			62.0	600				7.1	0.13		
			72.6	700			static	4.8	0.07		
			68.5	graded			HEPES	3.3	0.06		
			62.0	600				3.8	0.07		
	Zn	diamond	62.0	600		r-SBF	HEPES			45 ± 2	Li et al., 2020d

AZ61 (M16600; Mg 94%, Zn 4.8–6.2%, Zr ≥0.45%); AZ91D (8.3–9.7% Al, ≤0.03% Cu, ≤0.005% Fe, ≤0.002 Ni, 0.35–1.0% Zn, 0.15–0.5% Mn, ≤0.1 Si, 0.02% other metals); WE43 (UNS M18430; rare earths 2.4–4.4%, 3.7–4.2% Y, 0.4% Zr); ZK61 (Mg 93%, Al 6%, Zn 1%); DMEM, Dulbecco's Modified Eagle's Medium ($NaHCO_3$-buffered with sodium pyruvate and L-glutamine); HANKS, sodium bicarbonate-buffered salt solution (0.35 g/L $NaHCO_3$, 1 g/L glucose); SBF (142 mM Na^+, 5 mM K^+, 1.5 mM Mg^+, 2.5 mM Ca^{2+}, 148.8 mM Cl^-, 4.2 mM HCO_3^-, 1 mM HPO_4^{2-}, TRIS–buffered) (Kokubo and Takadama, 2006); r-SBF (HEPES-buffered SBF with 103 mM Cl^-, 27 mM HCO_3^-, and additional 0.5 mM SO_4^{2-}) (Oyane et al., 2003). CRI, Corrosion rates determined gravimetrically from immersion tests; CRE, Corrosion rates determined electrochemically. Tests requirements: bone substitute, not known; bone fixature < 0.5 mm/year (Chen et al., 2014); stents < 0.02 mm/year (Bowen et al., 2013).

slowly, recent efforts were mainly directed toward tuning their corrosion behavior by alloying. This may lead to grain refinement to improve degradation resistance of Mg, but can generate second phase(s) or cause grain boundary segregation, both of which can accelerate galvanic degradation. Biodegradation rate of SLM Mg was reduced by alloying with 1% Sn, while higher percentages of tin increased corrosion rates likely due to second phase(s) overshadowing the grain refinement effects (Zhou et al., 2016). Similar results are reported for SLM ZK30 (Shuai et al., 2018a). However, alloying Mg with aluminum (Al), like in AZ91 (8.3–9.7% Al) or AZ31B (2.5–3.5% Al), reduces its corrosion rate at the expense of its biocompatibility (Ghosh et al., 2020). A comparison of degradation rates of Fe-, Zn-, and Mg-based alloys (including AZ31B) was recently published, illustrating the improved corrosion resistance of Mg0.8Ca and Mg1Zn (Mei et al., 2020).

Corrosion rates of Fe-Mn alloys are reported to be higher than those of AM pure Fe (Li et al., 2019b; Shuai et al., 2020) because of increased galvanic degradation. Fe-20Mn was recently reported to have a decreased corrosion rate as compared to the pure metal, though (Mei et al., 2020). Addition of silver to Zn increased its corrosion rate, while, interestingly, addition of Mg to Zn either decreased or increased it, probably due to concentration-dependent different impacts of grain refinement and second phase (Shuai et al., 2018c; Yang Y. et al., 2018; Mei et al., 2020).

Impact of the Composition of the Test Solution on Corrosion Behavior

Published discrepancies between absorbable metal corrosion behavior likely result from non-comparable test conditions (Mei et al., 2020). To mimic human body physiology, it remains meaningful to use buffers to keep pH values constant (Törne et al., 2017). The addition of buffers like HEPES, however, can destabilize protective layers and accelerate Mg degradation by a magnitude. In absence of corrosion accelerating Tris–HCl, formation of uniform protective corrosion product layers slows corrosion rates in DMEM as compared to SBF (Liu et al., 2019). Using HEPES promoted the formation of passive layers in NaCl solution to reduce corrosion rates, while it showed opposite effects in SBF (Liu et al., 2019).

Of the few studies comparing the corrosion rates of these metals directly under similar conditions, a recent study analyzed all three metals in two simulated physiological solutions, and reported their exact composition for the 28-day immersion tests (Dong et al., 2021). In essence, corrosion rate was initially slower in Dulbecco's Modified Eagle's Medium (DMEM) for all three metals, with Mg showing the fastest burst corrosion rate in both SBF and DMEM. Intriguingly, the ranking of the relative corrosion speed changed over time, showing an increasing corrosion resistance of Mg after the initial 24 h, which confirms earlier data (Li et al., 2018b, 2020a). Typically, the corrosion rate of Mg is decreased as a function of increasing complexity of the medium, which indicates an urgent need to develop standard protocols for corrosion tests of absorbable metals (Mei et al., 2020). With a focus on Mg, recently a selection guide for corrosion media for absorbable metals, summarizing their advantages and shortcomings, was reported (Mei et al., 2020).

Design- and Post Manufacturing-Dependent Corrosion Aspects

Bone tissue is characterized by a gradual change in porosity from the outer cortical, compact bone toward an inner spongy tissue, with long bones being typical examples. This porosity and directionality is highly graded and dependent on local mechanical stimuli (e.g., strain energy density) (Campoli et al., 2012; Christen et al., 2013; Hazrati Marangalou et al., 2013; Zadpoor et al., 2013; Geraldes and Phillips, 2014; Nune et al., 2016). It is tempting to mimic these natural structures in AM porous implants as they will eventually be surrounded by new bony tissue of similar micro-architecture and biomechanical characteristics (Nune et al., 2016; Zhang X.-Y. et al., 2019).

AM porous absorbable metals showed a strongly location-dependent corrosion behavior. The core of cylindrical AM porous Mg implants corroded much more prominently than their periphery (Li et al., 2018b); potentially due to limited diffusion upon accumulation of degradation products within the narrow spaces between struts, where Mg ions locally may cause crevice-like corrosion. In contrast, AM porous Zn corroded primarily localized in a contact zone with the reaction vial, likely due to hindered diffusion (Li et al., 2020c). Despite further identical designs and testing methods, *in vitro* degradation of AM porous Fe occurred more prominently on its periphery than in its core (**Figures 1C**; Li et al., 2018a). We recently used geometrical design to control biodegradation of SLM porous Fe to show that corrosion rates were directly proportional to its porosity. Furthermore, its biodegradation profiles could be tuned using functionally graded designs (Li et al., 2019a). This was later confirmed for Zn (Li et al., 2020c), underscoring the importance of rational design strategies for AM PAM implants (**Table 1**).

Similar to inert AM porous metals, yield strengths and elastic modulus of AM PAMs are directly related to their porosity through a power law (Li et al., 2019a, 2020c). Two types of unit cells are prevalent: (i) lattice structures and (ii) sheet-based structures (**Figure 1C**) such as minimal surface designs (Zadpoor, 2019a). The former can be subdivided into bending- and stretch-dominated structures; with bending-dominated types generally having a higher energy absorption ability, while the latter structures show higher stiffnesses and yield strengths (Deshpande et al., 2001; Zadpoor, 2019b). SLM porous Fe cubic unit cell-based designs possess higher yield strengths than diamond unit cell types (Li et al., 2018a; Shuai et al., 2020). AM Zn of constant porosity also showed unit cell-dependent mechanical properties (Lietaert et al., 2020), but unit cell types also likely determine failure modes of scaffolds under compression (Mazur et al., 2016; Bobbert et al., 2017). SLM-based AM of functionally graded porous Fe and Zn of precisely controlled geometries were reviewed (Li et al., 2020a), realizing implants of trabecular bone-like mechanical properties

(Li et al., 2019a, 2020c). Fatigue cracks tend to initiate at junctions between two struts where stress concentration occurs under compression, when using a diamond unit cell design (Li et al., 2019b,c, 2020b). Graded structural design could increase fatigue strengths of SLM porous Zn (Li et al., 2020b), confirming earlier results for functionally graded porous EBM Ti-6Al-4V (Zhao et al., 2018).

Surface roughness likely affects corrosion rates of absorbable metals, too (Walter et al., 2013). As porous PBF implants often suffer from adhered powder particles loosely sintered to their struts, smoothening their surfaces can alter corrosion profiles, especially during the initial phase. Chemical etching or sandblasting are frequently used for polishing (Li et al., 2018a,b; Wen et al., 2018a,b), which may decrease their compressive mechanical properties (Hermawan, 2018; Li et al., 2018b). Sandblasting was found to improve fatigue resistance of inert AM porous titanium (Ahmadi et al., 2019). However, most surface treatment procedures fail to yield smooth homogeneous surfaces on both the periphery and inside the core of a porous implant (Li et al., 2018b, 2019a), stressing the importance of sophisticated quality control. Sandblasting can further induce compressive stresses under the surface, which may affect corrosion rates, too. Heat treatment increased degradation rates of AM WE43, but PEO coating seemed to decrease it (Kopp et al., 2019), and vacuum annealing increased yield strength of SLM Fe (Song et al., 2014b). Overall, AM processes may cause unique defects and microstructures, affecting their corrosion profile over time. Contrary to Mg, smaller grains of SLM Fe increased its corrosion rate as compared to cold-rolled Fe with larger grains (Li et al., 2018a), as the relationship between grain size and corrosion rate may dependent on the level of passivity on the metal surface (Ralston et al., 2010). Logically, HA coating on AM Fe scaffolds decreased its ion release during *in vitro* biodegradation (Yang C. et al., 2018). Of note, different AM process parameters result in different grain structures, which may also affect corrosion rates as shown for SLM Zn fabricated at different scanning speeds (Qin et al., 2020). Zn corrosion seems to increase with refined grain sizes due to higher grain boundary densities (Osorio et al., 2005; Qin et al., 2020), while nanocrystalline Zn provides apparent degradation resistance (Youssef et al., 2004). Additionally, AM-related residual internal stresses can affect degradation rates as well (Li et al., 2020a).

Biocompatibility and Clinical Application Potential

Significant amounts of the body's Mg and Zn content are stored in the inorganic bone matrix. The daily recommended intake of Mg is about 40–45 times higher than that of iron and zinc (Habibovic and Barralet, 2011; Florencio-Silva et al., 2015), suggesting its good tolerability (**Figure 1B**). Current clinical applications of magnesium-based implants in Orthopedics were recently reviewed comprehensively (Wang et al., 2020).

Several *in vitro* studies, as well as small animal studies, reported promising results on using iron as scaffolding material for cardiovascular and Orthopedic applications (Li et al., 2020a). Also a recent large animal model using iron-based degradable sponge-like implants manufactured by a powder metallurgical replication method underscored its potential for self-degrading, high load-bearing bone replacements (Wegener et al., 2020). Smart designs can further increase corrosion rates of Fe toward avoiding long-term side effects (Rahim et al., 2018), but own studies on porous SLM iron implants prompt to caution (Li et al., 2018a, 2020a). Corroding iron fragments are further known to migrate through the body, causing chronic inflammation (Rahim et al., 2018).

Zinc alloys with favorable corrosion kinetics and biocompatible degradation products hold several promises for e.g., stent applications (Rahim et al., 2018).

Appropriately modified magnesium-based implants are already marketed for cardiovascular applications (e.g., stents) and Orthopedic applications (e.g., compression or interference screws) and recent studies claimed they are resorbed to 95% within a year (Rahim et al., 2018). To better predict their translational potential, improved standards are not only needed for corrosion testing, but also for assessing their cytocompatibility *in vitro*. Recommendations to improve ISO 10993-5/-12 for Mg (Jung et al., 2019), and a recent technical corrigendum to ISO 10993-1:2009 (i.e., ISO 10993-1:2018) now containing additional information on the evaluation of, among others, absorbable materials, are important steps to facilitate the translational development of novel absorbable biomaterials.

A series of identically designed cylindrical porous SLM implants were used to systematically evaluate the cytotoxicity of pure Zn, WE43, and pure Fe, using the same osteoblast-like cells and identical assays (Li et al., 2018a, 2019a, 2020d) to reveal a decreasing cytocompatibility in this order under these conditions. Like with corrosion testing, present cytocompatibility studies are hardly comparable. Limitations of most current studies further include very short *in vitro* evaluation periods and highly cell type-dependent outcomes (Li et al., 2020a).

In summary, SLM Fe appears to be relatively cytotoxic (Li et al., 2018a), potentially limiting its applications, while pure porous Mg corrodes fast (Hermawan, 2018). Currently, Zn and its alloys, seems to have an intermediate absorption rate and a reasonable cytocompatibility, which is currently based on only a handful of reports (**Table 1**), primarily in a cardiovascular context (Bowen et al., 2016; Drelich et al., 2017; Levy et al., 2017).

DISCUSSION

Mg and its alloys have a higher strength as compared to native bone, but a Young's modulus closely matching that of cortical bone. Such properties overcome shortcomings of traditional metallic and polymeric biomaterials (Wang et al., 2020) in Orthopedics: polymers are often too weak, and solid metals like titanium (Ti), iron (red) or steel (CoCr) are too stiff to mimic the mechanical properties of bone, while ceramics (Al_2O_3 or ZrO_2) are too brittle for fully load-bearing implants in humans (**Table 1** and **Figure 1**; Li et al., 2020a).

Other recent review articles focused on the design and degradation (Shuai et al., 2019b; Li et al., 2020a) of absorbable Orthopedic implants, corrosion testing methods (Mei et al., 2020; Dong et al., 2021), biomaterial- stem cell interactions (Gao et al., 2017), the role of magnesium ions in bone repair (Wang et al., 2020), and the clinical translation of absorbable metals (Han et al., 2019; Wang et al., 2020).

In this mini review, we highlighted recent developments in SLM-based AM of PAM implants as they hold incredible potential to satisfy all basic functional requirements of an ideal bone-substituting implant. Their microstructural design holds a plethora of opportunities to fine-tune their corrosion behavior to specific clinical applications. To facilitate the transition from basic research into clinics, and to close remaining knowledge gaps in this rapidly evolving field, better standards for reporting corrosion test results and cytocompatibility data are needed though. Thus, a lot needs to be improved before widespread clinical application of such materials is feasible.

Due to lacking data, it is currently still largely unclear if *in vitro* corrosion rates of AM PAMs are by any means predictive of the *in vivo* situation. Next to reporting test solution details, it may be better to report weight loss percentages in future evaluations in addition to degradation rates as mm/year, because the latter unit makes more sense for bulk absorbable metals to which it is usually applied. For porous structures, the ratio of surface area to weight is much higher than for bulk counterparts and changes constantly during the degradation process. For bulk Mg, *in vitro* degradation rates are generally 1–4 times higher than values obtained *in vivo*, but are largely depending on the used alloy and *in vitro* testing conditions (Sanchez et al., 2015). To tune absorption rates of AM porous metals where needed, it is imperative to understand how *in vitro* corrosion is affected by chemical composition, microstructure, topological design, and surface conditions.

To improve mechanical properties, (i) Mg, Fe, and Zn alloys with higher mechanical properties need to be developed specifically for AM, (ii) as of yet underappreciated stretch-dominated or minimal surface designs as well as, and (iii) functionally graded structures combining different unit cell types and sizes should be considered. Transformation hardening may more likely work for Fe-based absorbable alloys than for Mg and Zn, or derivatives (Li et al., 2020a). As AM is a net-shape manufacturing technique, most strengthening mechanisms usually applied to bulk metals will not be applicable and accessibility inside 3D porous structures will be severely restricted. Rapid solidification during SLM results in finer grains, with size adjustment potential by layer-wise thermal history controlling. Process optimization and post-AM heat treatments may also improve mechanical properties. Alloying pure Fe with other elements might improve its biocompatibility, mechanical properties and biodegradation rate. Exploring Mg-based porous metallic glasses could result in AM Mg-based porous biomaterials with simultaneously improved corrosion resistance and mechanical properties. Zn-based mechanical properties may benefit from alloying Zn with other elements, particularly Mg and Ca. Better surface polishing methods and procedures are also needed (Li et al., 2020a). Creep and aging of AM Zn-based materials and their influences on the performance of these materials need to be further investigated. Different loading regimens (e.g., compression-tension, tension-tension, bending, and torsion) should be applied to all AM PAMs. Finally, future AM porous implants should not only consider *initial* bone-mimetic mechanical properties, but also anticipate dynamic changes during bone regeneration as well as parallel occurring deterioration of the implant properties. Thus, requiring much more sophisticated approaches.

This also holds for biocompatibility testing of novel implants, a detailed discussion of which is beyond our scope. However, good osteointegration would be a prerequisite to a successful clinical translation. As was shown for iron and zinc (Ray et al., 2018; Yang H. et al., 2018), novel coatings may be considered to potentially tune implant degradation and bone formation rates (Yu et al., 2017; Kang et al., 2019), too. It is envisioned that appropriate (functional) coatings will improve bone-forming abilities of all future AM PAMs. The few current *in vivo* studies unanimously reported new bone formation around SLM porous absorbable metal implants, but longer studies are desirable (Wang et al., 2020).

The "materialome" should be established to guide novel developments instead of pursuing a trial-and-error approach; (ii) the influence of the geometrical design on mechanical properties, corrosion behavior, cell-material-adhesion, and osseointegration should be systematically investigated by experimental and numerical approaches; (iii) the big gap between *in vitro* and *in vivo* results has to be closed. The plethora of educt and process parameters will become a serious challenge which may require real-time monitoring of the melt pool and powder bed *in situ* (Li et al., 2020a).

General recommendations for potentially interesting future work include (i) considering machine learning approaches to improve the selection of the process parameters and to better appreciate the complex relationships between chemical composition, lattice structure geometry, processing parameters, microstructure, and the resulting mechanical properties. A bright future awaits SLM porous absorbable metal implants when satisfying basic functional requirements of an ideal bone-substitute becomes achievable. Yet, more sophisticated round-robin evaluations are required to close current gaps in our knowledge.

AUTHOR CONTRIBUTIONS

HJ drafted, revised the manuscript, and submitted the final version. YL, JZ, AZ, and K-US contributed specific sections and critically co-revised the manuscript. All authors read the final version and agreed to its submission.

FUNDING

This work was supported by the Federal Ministry of Education and Research (BMBF) and the Ministry of Culture and Science

of the State of North Rhine-Westphalia (MKW) under the Excellence Strategy of the Federal Government and the Länder (OPSF597). Financial support from the PRosPERoS project, funded by the Interreg VA Flanders –Netherlands Program (CCI grant no. 2014TC16RFCB046), and the Medical Faculty (IZKF) of the RWTH Aachen University is also acknowledged.

REFERENCES

Ahmadi, S. M., Hedayati, R., Li, Y., Lietaert, K., Tümer, N., Fatemi, A., et al. (2018). Fatigue performance of additively manufactured meta-biomaterials: the effects of topology and material type. *Acta Biomater.* 65, 292–304. doi: 10.1016/j.actbio.2017.11.014

Ahmadi, S. M., Kumar, R., Borisov, E. V., Petrov, R., Leeflang, S., Li, Y., et al. (2019). From microstructural design to surface engineering: a tailored approach for improving fatigue life of additively manufactured meta-biomaterials. *Acta Biomater.* 83, 153–166. doi: 10.1016/j.actbio.2018.10.043

Allsopp, B. J., Hunter-Smith, D. J., and Rozen, W. M. (2016). Vascularized versus nonvascularized bone grafts: what is the evidence? *Clin. Orthop. Relat. Res.* 474, 1319–1327. doi: 10.1007/s11999-016-4769-4

Amin Yavari, S., van der Stok, J., Weinans, H., and Zadpoor, A. A. (2013). Full-field strain measurement and fracture analysis of rat femora in compression test. *J. Biomech.* 46, 1282–1292. doi: 10.1016/j.jbiomech.2013.02.007

Bobbert, F. S. L., Lietaert, K., Eftekhari, A. A., Pouran, B., Ahmadi, S. M., Weinans, H., et al. (2017). Additively manufactured metallic porous biomaterials based on minimal surfaces: a unique combination of topological, mechanical, and mass transport properties. *Acta Biomater.* 53, 572–584. doi: 10.1016/j.actbio.2017.02.024

Bowen, P. K., Drelich, J., and Goldman, J. (2013). Zinc exhibits ideal physiological corrosion behavior for bioabsorbable stents. *Adv. Mater.* 25, 2577–2582. doi: 10.1002/adma.201300226

Bowen, P. K., Shearier, E. R., Zhao, S., Guillory, R. J., Zhao, F., Goldman, J., et al. (2016). Biodegradable metals for cardiovascular stents: from clinical concerns to recent Zn-alloys. *Adv. Healthc. Mater.* 5, 1121–1140. doi: 10.1002/adhm.201501019

Campoli, G., Weinans, H., and Zadpoor, A. A. (2012). Computational load estimation of the femur. *J. Mech. Behav. Biomed. Mater.* 10, 108–119. doi: 10.1016/j.jmbbm.2012.02.011

Carluccio, D., Bermingham, M., Kent, D., Demir, A. G., Previtali, B., and Dargusch, M. S. (2019). Comparative study of pure iron manufactured by selective laser melting, laser metal deposition, and casting processes. *Adv. Eng. Mater.* 21:1900049. doi: 10.1002/adem.201900049

Carluccio, D., Xu, C., Venezuela, J., Cao, Y., Kent, D., Bermingham, M., et al. (2020). Additively manufactured iron-manganese for biodegradable porous load-bearing bone scaffold applications. *Acta Biomater.* 103, 346–360. doi: 10.1016/j.actbio.2019.12.018

Chen, Q., and Thouas, G. A. (2015). Metallic implant biomaterials. *Mater. Sci. Eng. R Rep.* 87, 1–57. doi: 10.1016/j.mser.2014.10.001

Chen, Y., Xu, Z., Smith, C., and Sankar, J. (2014). Recent advances on the development of magnesium alloys for biodegradable implants. *Acta Biomater.* 10, 4561–4573. doi: 10.1016/j.actbio.2014.07.005

Christen, P., Ito, K., Knippels, I., Müller, R., van Lenthe, G. H., and van Rietbergen, B. (2013). Subject-specific bone loading estimation in the human distal radius. *J. Biomech.* 46, 759–766. doi: 10.1016/j.jbiomech.2012.11.016

DebRoy, T., Wei, H. L., Zuback, J. S., Mukherjee, T., Elmer, J. W., Milewski, J. O., et al. (2018). Additive manufacturing of metallic components – process, structure and properties. *Prog. Mater. Sci.* 92, 112–224.

Deshpande, V. S., Ashby, M., and Fleck, N. (2001). Foam topology: Bending versus stretching dominated architectures. *Acta Mater.* 49, 1035–1040. doi: 10.1016/s1359-6454(00)00379-7

Dimitriou, R., Jones, E., McGonagle, D., and Giannoudis, P. V. (2011). Bone regeneration: current concepts and future directions. *BMC Med.* 9:66.

Do, A. V., Khorsand, B., Geary, S. M., and Salem, A. K. (2015). 3D printing of scaffolds for tissue regeneration applications. *Adv. Healthc Mater.* 4, 1742–1762. doi: 10.1002/adhm.201500168

Dong, H., Lin, F., Boccaccini, A. R., and Virtanen, S. (2021). Corrosion behavior of biodegradable metals in two different simulated physiological solutions: comparison of Mg, Zn and Fe. *Corrosion Sci.* 182:109278. doi: 10.1016/j.corsci.2021.109278

Drelich, A. J., Zhao, S., Guillory, R. J., Drelich, J. W., and Goldman, J. (2017). Long-term surveillance of zinc implant in murine artery: Surprisingly steady biocorrosion rate. *Acta Biomater.* 58, 539–549. doi: 10.1016/j.actbio.2017.05.045

Fayaz, H. C., Jupiter, J. B., Pape, H. C., Smith, R. M., Giannoudis, P. V., Moran, C. G., et al. (2011). Challenges and barriers to improving care of the musculoskeletal patient of the future - a debate article and global perspective. *Patient Saf. Surg.* 5:23. doi: 10.1186/1754-9493-5-23

Florencio-Silva, R., Sasso, G. R., Sasso-Cerri, E., Simões, M. J., and Cerri, P. S. (2015). Biology of bone tissue: structure, function, and factors that influence bone cells. *Biomed. Res. Int.* 2015:421746.

Francis, A., Yang, Y., Virtanen, S., and Boccaccini, A. R. (2015). Iron and iron-based alloys for temporary cardiovascular applications. *J. Mater. Sci. Mater. Med.* 26:138.

Gao, C., Peng, S., Feng, P., and Shuai, C. (2017). Bone biomaterials and interactions with stem cells. *Bone Res.* 5:17059.

Gao, C., Yao, M., Li, S., Feng, P., Peng, S., and Shuai, C. (2019). Highly biodegradable and bioactive Fe-Pd-bredigite biocomposites prepared by selective laser melting. *J. Adv. Res.* 20, 91–104. doi: 10.1016/j.jare.2019.06.001

Geetha, M., Singh, A. K., Asokamani, R., and Gogia, A. K. (2009). Ti based biomaterials, the ultimate choice for orthopaedic implants – a review. *Prog. Mater. Sci.* 54, 397–425. doi: 10.1016/j.pmatsci.2008.06.004

Geraldes, D. M., and Phillips, A. T. (2014). A comparative study of orthotropic and isotropic bone adaptation in the femur. *Int. J. Numer. Method Biomed. Eng.* 30, 873–889. doi: 10.1002/cnm.2633

Ghosh, M., Hartmann, H., Jakobi, M., März, L., Bichmann, L., Freudenmann, L. K., et al. (2020). The Impact of Biomaterial Cell Contact on the Immunopeptidome. *Front. Bioeng. Biotechnol.* 8:571294.

Giedraitis, A., Arnoczky, S. P., and Bedi, A. (2014). Allografts in soft tissue reconstructive procedures: important considerations. *Sports Health* 6, 256–264. doi: 10.1177/1941738113503442

Habibovic, P., and Barralet, J. E. (2011). Bioinorganics and biomaterials: bone repair. *Acta Biomater.* 7, 3013–3026. doi: 10.1016/j.actbio.2011.03.027

Han, H.-S., Loffredo, S., Jun, I., Edwards, J., Kim, Y.-C., Seok, H.-K., et al. (2019). Current status and outlook on the clinical translation of biodegradable metals. *Mater. Today* 23, 57–71. doi: 10.1016/j.mattod.2018.05.018

Hazrati Marangalou, J., Ito, K., Cataldi, M., Taddei, F., and van Rietbergen, B. (2013). A novel approach to estimate trabecular bone anisotropy using a database approach. *J. Biomech.* 46, 2356–2362. doi: 10.1016/j.jbiomech.2013.07.042

He, C., Bin, S., Wu, P., Gao, C., Feng, P., Yang, Y., et al. (2017). Microstructure evolution and biodegradation behavior of laser rapid solidified Mg–Al–Zn alloy. *Metals* 7:105. doi: 10.3390/met7030105

Hermawan, H. (2018). Updates on the research and development of absorbable metals for biomedical applications. *Prog. Biomater.* 7, 93–110. doi: 10.1007/s40204-018-0091-4

Hexter, A. T., Hislop, S. M., Blunn, G. W., and Liddle, A. D. (2018). The effect of bearing surface on risk of periprosthetic joint infection in total hip arthroplasty: a systematic review and meta-analysis. *Bone Joint J.* 100-B, 134–142. doi: 10.1302/0301-620x.100b2.bjj-2017-0575.r1

Jung, O., Smeets, R., Hartjen, P., Schnettler, R., Feyerabend, F., Klein, M., et al. (2019). Improved in vitro test procedure for full assessment of the cytocompatibility of degradable magnesium based on ISO 10993-5/-12. *Int. J. Mol. Sci.* 20:255. doi: 10.3390/ijms20020255

Kang, M.-H., Lee, H., Jang, T.-S., Seong, Y.-J., Kim, H.-E., Koh, Y.-H., et al. (2019). Biomimetic porous Mg with tunable mechanical properties and biodegradation rates for bone regeneration. *Acta Biomater.* 84, 453–467. doi: 10.1016/j.actbio.2018.11.045

Kokubo, T., and Takadama, H. (2006). How useful is SBF in predicting in vivo bone bioactivity? *Biomaterials* 27, 2907–2915. doi: 10.1016/j.biomaterials.2006.01.017

Kopp, A., Derra, T., Müther, M., Jauer, L., Schleifenbaum, J. H., Voshage, M., et al. (2019). Influence of design and postprocessing parameters on the degradation behavior and mechanical properties of additively manufactured magnesium scaffolds. *Acta Biomater.* 98, 23–35. doi: 10.1016/j.actbio.2019.04.012

Kruth, J. P., Froyen, L., Van Vaerenbergh, J., Mercelis, P., Rombouts, M., and Lauwers, B. (2004). Selective laser melting of iron-based powder. *J. Mater. Process. Technol.* 149, 616–622. doi: 10.1016/j.jmatprotec.2003.11.051

Levy, G. K., Goldman, J., and Aghion, E. (2017). The prospects of zinc as a structural material for biodegradable implants- a review paper. *Metals* 7, 1–18. doi: 10.1016/j.actbio.2019.12.023

Li, Y., Jahr, H., Lietaert, K., Pavanram, P., Yilmaz, A., Fockaert, L. I., et al. (2018a). Additively manufactured biodegradable porous iron. *Acta Biomater.* 77, 380–393. doi: 10.1016/j.actbio.2018.07.011

Li, Y., Jahr, H., Pavanram, P., Bobbert, F. S. L., Puggi, U., Zhang, X. Y., et al. (2019a). Additively manufactured functionally graded biodegradable porous iron. *Acta Biomater.* 96, 646–661. doi: 10.1016/j.actbio.2019.11.040

Li, Y., Jahr, H., Zhang, X. Y., Leeflang, M. A., Li, W., Pouran, B., et al. (2019b). Biodegradation-affected fatigue behavior of additively manufactured porous magnesium. *Addit. Manuf.* 28, 299–311. doi: 10.1016/j.addma.2019.05.013

Li, Y., Jahr, H., Zhou, J., and Zadpoor, A. A. (2020a). Additively manufactured biodegradable porous metals. *Acta Biomater.* 115, 29–50. doi: 10.1016/j.actbio.2020.08.018

Li, Y., Li, W., Bobbert, F. S. L., Lietaert, K., Dong, J. H., Leeflang, M. A., et al. (2020b). Corrosion fatigue behavior of additively manufactured biodegradable porous zinc. *Acta Biomater.* 106, 439–449. doi: 10.1016/j.actbio.2020.02.001

Li, Y., Lietaert, K., Li, W., Zhang, X. Y., Leeflang, M. A., Zhou, J., et al. (2019c). Corrosion fatigue behavior of additively manufactured biodegradable porous iron. *Corrosion Sci.* 156, 106–116. doi: 10.1016/j.corsci.2019.05.003

Li, Y., Pavanram, P., Zhou, J., Lietaert, K., Bobbert, F. S. L., Kubo, Y., et al. (2020c). Additively manufactured functionally graded biodegradable porous zinc. *Biomater. Sci.* 8, 2404–2419. doi: 10.1039/c9bm01904a

Li, Y., Pavanram, P., Zhou, J., Lietaert, K., Taheri, P., Li, W., et al. (2020d). Additively manufactured biodegradable porous zinc. *Acta Biomater.* 101, 609–623. doi: 10.1016/j.actbio.2019.10.034

Li, Y., Zhou, J., Pavanram, P., Leeflang, M. A., Fockaert, L. I., Pouran, B., et al. (2018b). Additively manufactured biodegradable porous magnesium. *Acta Biomater.* 67, 378–392. doi: 10.1016/j.actbio.2017.12.008

Lietaert, K., Zadpoor, A. A., Sonnaert, M., Schrooten, J., Weber, L., Mortensen, A., et al. (2020). Mechanical properties and cytocompatibility of dense and porous Zn produced by laser powder bed fusion for biodegradable implant applications. *Acta Biomater.* 110, 289–302. doi: 10.1016/j.actbio.2020.04.006

Liu, X., and Ma, P. X. (2004). Polymeric scaffolds for bone tissue engineering. *Ann. Biomed. Eng.* 32, 477–486. doi: 10.1023/b:abme.0000017544.36001.8e

Liu, X., Yang, H., Xiong, P., Li, W., Huang, H.-H., and Zheng, Y. (2019). Comparative studies of Tris-HCl, HEPES and NaHCO3/CO2 buffer systems on the biodegradation behaviour of pure Zn in NaCl and SBF solutions. *Corrosion Sci.* 157, 205–219. doi: 10.1016/j.corsci.2019.05.018

Liu, Y., Zheng, Y., and Hayes, B. (2017). Degradable, absorbable or resorbable–what is the best grammatical modifier for an implant that is eventually absorbed by the body? *Sci. Chin. Mater.* 60, 377–379. doi: 10.1007/s40843-017-9023-9

Loi, F., Córdova, L. A., Pajarinen, J., Lin, T. H., Yao, Z., and Goodman, S. B. (2016). Inflammation, fracture and bone repair. *Bone* 86, 119–130. doi: 10.1016/j.bone.2016.02.020

Manakari, V., Parande, G., and Gupta, M. (2016). Selective laser melting of magnesium and magnesium alloy powders: a review. *Metals* 7:2. doi: 10.3390/met7010002

Marian, M., and Sacks, G. (2009). Micronutrients and older adults. *Nutr. Clin. Pract.* 24, 179–195. doi: 10.1177/0884533609332177

Matassi, F., Botti, A., Sirleo, L., Carulli, C., and Innocenti, M. (2013). Porous metal for orthopedics implants. *Clin. Cases Mineral Bone Metab.* 10, 111–115.

Mazur, M., Leary, M., Sun, S., Vcelka, M., Shidid, D. P., and Brandt, M. (2016). Deformation and failure behaviour of Ti-6Al-4V lattice structures manufactured by selective laser melting (SLM). *Int. J. Adv. Manuf. Technol.* 84, 1391–1411.

Mei, D., Lamaka, S. V., Lu, X., and Zheludkevich, M. L. (2020). Selecting medium for corrosion testing of bioabsorbable magnesium and other metals – a critical review. *Corrosion Sci.* 171:108722. doi: 10.1016/j.corsci.2020.108722

Montani, M., Demir, A. G., Mostaed, E., Vedani, M., and Previtali, B. (2017). Processability of pure Zn and pure Fe by SLM for biodegradable metallic implant manufacturing. *Rapid Prototyping J.* 23, 514–523. doi: 10.1108/rpj-08-2015-0100

Mostaed, E., Sikora-Jasinska, M., Drelich, J. W., and Vedani, M. (2018). Zinc-based alloys for degradable vascular stent applications. *Acta Biomater.* 71, 1–23. doi: 10.1016/j.actbio.2018.03.005

Ng, C. C., Savalani, M., and Man, H. C. (2011b). Fabrication of magnesium using selective laser melting technique. *Rapid Prototyping J.* 17, 479–490. doi: 10.1108/13552541111184206

Ng, C. C., Savalani, M. M., Lau, M. L., and Man, H. C. (2011a). Microstructure and mechanical properties of selective laser melted magnesium. *Appl. Surf. Sci.* 257, 7447–7454. doi: 10.1016/j.apsusc.2011.03.004

Nune, K. C., Kumar, A., Misra, R. D., Li, S. J., Hao, Y. L., and Yang, R. (2016). Osteoblast functions in functionally graded Ti-6Al-4 V mesh structures. *J. Biomater. Appl.* 30, 1182–1204. doi: 10.1177/0885328215617868

Oh, I.-H., Nomura, N., Masahashi, N., and Hanada, S. (2003). Mechanical properties of porous titanium compacts prepared by powder sintering. *Scripta Mater.* 49, 1197–1202. doi: 10.1016/j.scriptamat.2003.08.018

Oryan, A., Alidadi, S., Moshiri, A., and Maffulli, N. (2014). Bone regenerative medicine: classic options, novel strategies, and future directions. *J. Orthopaedic Surg. Res.* 9:18. doi: 10.1186/1749-799x-9-18

Osorio, W., Freire, C., and Garcia, A. (2005). The role of macrostructural morphology and grain size on the corrosion resistance of Zn and Al castings. *Mater. Sci. Eng. A* 402, 22–32. doi: 10.1016/j.msea.2005.02.094

Oyane, A., Onuma, K., Ito, A., Kim, H. M., Kokubo, T., and Nakamura, T. (2003). Formation and growth of clusters in conventional and new kinds of simulated body fluids. *J. Biomed. Mater. Res. A* 64, 339–348. doi: 10.1002/jbm.a.10426

Polaris Market Research (2020). *Bone Grafts and Substitutes Market Size, Share & Trends Analysis Report By Material Type (Natural, Synthetic); By Application Type (Spinal Fusion, Craniomaxillofacial, Long Bone); By Region*. New York, NY: Polaris Market Research.

Qin, Y., Wen, P., Guo, H., Xia, D., Zheng, Y., Jauer, L., et al. (2019). Additive manufacturing of biodegradable metals: current research status and future perspectives. *Acta Biomater.* 98, 3–22. doi: 10.1016/j.actbio.2019.04.046

Qin, Y., Wen, P., Xia, D., Guo, H., Voshage, M., Jauer, L., et al. (2020). Effect of grain structure on the mechanical properties and in vitro corrosion behavior of additively manufactured pure Zn. *Addit. Manuf.* 33:101134. doi: 10.1016/j.addma.2020.101134

Rahim, M. I., Ullah, S., and Mueller, P. P. (2018). Advances and challenges of biodegradable implant materials with a focus on magnesium-alloys and bacterial infections. *Metals* 8:532. doi: 10.3390/met8070532

Ralston, K. D., Birbilis, N., and Davies, C. H. J. (2010). Revealing the relationship between grain size and corrosion rate of metals. *Scripta Mater.* 63, 1201–1204. doi: 10.1016/j.scriptamat.2010.08.035

Ray, S., Thormann, U., Eichelroth, M., Budak, M., Biehl, C., Rupp, M., et al. (2018). Strontium and bisphosphonate coated iron foam scaffolds for osteoporotic fracture defect healing. *Biomaterials* 157, 1–16. doi: 10.1016/j.biomaterials.2017.11.049

Sanchez, A. H. M., Luthringer, B. J. C., Feyerabend, F., and Willumeit, R. (2015). Mg and Mg alloys: how comparable are in vitro and in vivo corrosion rates? A review. *Acta Biomater.* 13, 16–31. doi: 10.1016/j.actbio.2014.11.048

Seitz, H., Rieder, W., Irsen, S., Leukers, B., and Tille, C. (2005). Three-dimensional printing of porous ceramic scaffolds for bone tissue engineering. *J. Biomed. Mater. Res. B Appl. Biomater.* 74, 782–788.

Shuai, C., Cheng, Y., Yang, Y., Peng, S., Yang, W., and Qi, F. (2019a). Laser additive manufacturing of Zn-2Al part for bone repair: Formability, microstructure and properties. *J. Alloys Compd.* 798, 606–615. doi: 10.1016/j.jallcom.2019.05.278

Shuai, C., He, C., Feng, P., Guo, W., Gao, C., Wu, P., et al. (2018a). Biodegradation mechanisms of selective laser-melted Mg–xAl–Zn alloy: grain size and intermetallic phase. *Virtual Phys. Prototyping* 13, 59–69. doi: 10.1080/17452759.2017.1408918

Shuai, C., Li, S., Peng, S., Feng, P., Lai, Y., and Gao, C. (2019b). Biodegradable metallic bone implants. *Mater. Chem. Front.* 3, 544–562. doi: 10.1039/c8qm00507a

Shuai, C., Liu, L., Zhao, M., Feng, P., Yang, Y., Guo, W., et al. (2018b). Microstructure, biodegradation, antibacterial and mechanical properties of

ZK60-Cu alloys prepared by selective laser melting technique. *J. Mater. Sci. Technol.* 34, 1944–1952. doi: 10.1016/j.jmst.2018.02.006

Shuai, C., Xue, L., Gao, C., Yang, Y., Peng, S., and Zhang, Y. (2018c). Selective laser melting of Zn–Ag alloys for bone repair: microstructure, mechanical properties and degradation behaviour. *Virtual Phys. Prototyping* 13, 146–154. doi: 10.1080/17452759.2018.1458991

Shuai, C., Yang, W., Yang, Y., Pan, H., He, C., Qi, F., et al. (2020). Selective laser melted Fe-Mn bone scaffold: microstructure, corrosion behavior and cell response. *Mater. Res. Express* 7:015404. doi: 10.1088/2053-1591/ab62f5

Song, B., Dong, S., Deng, S., Liao, H., and Coddet, C. (2014a). Microstructure and tensile properties of iron parts fabricated by selective laser melting. *Optics Laser Technol.* 56, 451–460. doi: 10.1016/j.optlastec.2013.09.017

Song, B., Dong, S., Liu, Q., Liao, H., and Coddet, C. (2014b). Vacuum heat treatment of iron parts produced by selective laser melting: microstructure, residual stress and tensile behavior. *Mater. Des.* 54, 727–733. doi: 10.1016/j.matdes.2013.08.085

Törne, K., Örnberg, A., and Weissenrieder, J. (2017). The influence of buffer system and biological fluids on the degradation of magnesium. *J. Biomed. Mater. Res. B Appl. Biomater.* 105, 1490–1502. doi: 10.1002/jbm.b.33685

Van der Stok, J., Van Lieshout, E. M., El-Massoudi, Y., Van Kralingen, G. H., and Patka, P. (2011). Bone substitutes in the Netherlands - a systematic literature review. *Acta Biomater.* 7, 739–750. doi: 10.1016/j.actbio.2010.07.035

Venezuela, J., and Dargusch, M. S. (2019). The influence of alloying and fabrication techniques on the mechanical properties, biodegradability and biocompatibility of zinc: A comprehensive review. *Acta Biomater.* 87, 1–40. doi: 10.1016/j.actbio.2019.01.035

Walter, R., Kannan, M. B., He, Y., and Sandham, A. (2013). Effect of surface roughness on the in vitro degradation behaviour of a biodegradable magnesium-based alloy. *Appl. Surface Sci.* 279, 343–348. doi: 10.1016/j.apsusc.2013.04.096

Wang, J. L., Xu, J. K., Hopkins, C., Chow, D. H., and Qin, L. (2020). Biodegradable magnesium-based implants in Orthopedics-A general review and perspectives. *Adv. Sci. (Weinh)* 7:1902443. doi: 10.1002/advs.201902443

Wang, W., and Yeung, K. W. K. (2017). Bone grafts and biomaterials substitutes for bone defect repair: a review. *Bioactive Mater.* 2, 224–247. doi: 10.1016/j.bioactmat.2017.05.007

Wegener, B., Sichler, A., Milz, S., Sprecher, C., Pieper, K., Hermanns, W., et al. (2020). Development of a novel biodegradable porous iron-based implant for bone replacement. *Sci. Rep.* 10:9141.

Wei, K., Gao, M., Wang, Z., and Zeng, X. (2014). Effect of energy input on formability, microstructure and mechanical properties of selective laser melted AZ91D magnesium alloy. *Mater. Sci. Eng. A* 611, 212–222. doi: 10.1016/j.msea.2014.05.092

Wei, K., Zeng, X., Wang, Z., Deng, J., Liu, M., Huang, G., et al. (2019). Selective laser melting of Mg-Zn binary alloys: effects of Zn content on densification behavior, microstructure, and mechanical property. *Mater. Sci. Eng. A* 756, 226–236. doi: 10.1016/j.msea.2019.04.067

Wen, C. E., Mabuchi, M., Yamada, Y., Shimojima, K., Chino, Y., and Asahina, T. (2001). Processing of biocompatible porous Ti and Mg. *Scripta Mater.* 45, 1147–1153. doi: 10.1016/s1359-6462(01)01132-0

Wen, P., Jauer, L., Voshage, M., Chen, Y., Poprawe, R., and Schleifenbaum, J. H. (2018a). Densification behavior of pure Zn metal parts produced by selective laser melting for manufacturing biodegradable implants. *J. Mater. Process. Technol.* 258, 128–137. doi: 10.1016/j.jmatprotec.2018.03.007

Wen, P., Voshage, M., Jauer, L., Chen, Y., Qin, Y., Poprawe, R., et al. (2018b). Laser additive manufacturing of Zn metal parts for biodegradable applications: Processing, formation quality and mechanical properties. *Mater. Des.* 155, 36–45. doi: 10.1016/j.matdes.2018.05.057

Witte, F., Jauer, L., Meiners, W., Kronbach, Z., Strohschein, K., and Schmidt, T. (2016). Open-porous biodegradable magnesium scaffolds produced by selective laser melting for individualized bone replacement. *Front. Bioeng. Biotechnol.* 4:708.

Wu, S., Liu, X., Yeung, K., Liu, C., and Yang, X. (2014). Biomimetic porous scaffolds for bone tissue engineering. *Mater. Sci. Eng. R Rep.* 80, 1–36. doi: 10.1016/j.mser.2014.04.001

Yan, Q., Dong, H., Su, J., Han, J., Song, B., Wei, Q., et al. (2018). A review of 3D printing technology for medical applications. *Engineering* 4, 729–742.

Yang, C., Huan, Z., Wang, X., Wu, C., and Chang, J. (2018). 3D PRINTED Fe scaffolds with HA nanocoating for bone regeneration. *ACS Biomater. Sci. Eng.* 4, 608–616. doi: 10.1021/acsbiomaterials.7b00885

Yang, H., Qu, X., Lin, W., Wang, C., Zhu, D., Dai, K., et al. (2018). In vitro and in vivo studies on zinc-hydroxyapatite composites as novel biodegradable metal matrix composite for orthopedic applications. *Acta Biomater.* 71, 200–214. doi: 10.1016/j.actbio.2018.03.007

Yang, Y., Yuan, F., Gao, C., Feng, P., Xue, L., He, S., et al. (2018). A combined strategy to enhance the properties of Zn by laser rapid solidification and laser alloying. *J. Mech. Behav. Biomed. Mater.* 82, 51–60. doi: 10.1016/j.jmbbm.2018.03.018

Youssef, K., Koch, C. C., and Fedkiw, P. (2004). Improved corrosion behavior of nanocrystalline zinc produced by pulse-current electrodeposition. *Corrosion Sci.* 46, 51–64. doi: 10.1016/s0010-938x(03)00142-2

Yu, W., Zhao, H., Ding, Z., Zhang, Z., Sun, B., Shen, J., et al. (2017). In vitro and in vivo evaluation of MgF2 coated AZ31 magnesium alloy porous scaffolds for bone regeneration. *Colloids Surf. B Biointerf.* 149, 330–340. doi: 10.1016/j.colsurfb.2016.10.037

Zadpoor, A. A. (2015). Bone tissue regeneration: the role of scaffold geometry. *Biomater. Sci.* 3, 231–245. doi: 10.1039/c4bm00291a

Zadpoor, A. A. (2019a). Additively manufactured porous metallic biomaterials. *J. Mater. Chem. B* 7, 4088–4117. doi: 10.1039/c9tb00420c

Zadpoor, A. A. (2019b). Mechanical performance of additively manufactured meta-biomaterials. *Acta Biomater.* 85, 41–59. doi: 10.1016/j.actbio.2018.12.038

Zadpoor, A. A., Campoli, G., and Weinans, H. (2013). Neural network prediction of load from the morphology of trabecular bone. *Appl. Math. Model.* 37, 5260–5276. doi: 10.1016/j.apm.2012.10.049

Zhang, L., Yang, G., Johnson, B. N., and Jia, X. (2019). Three-dimensional (3D) printed scaffold and material selection for bone repair. *Acta Biomater.* 84, 16–33. doi: 10.1016/j.actbio.2018.11.039

Zhang, X.-Y., Fang, G., Leeflang, S., Zadpoor, A. A., and Zhou, J. (2019). Topological design, permeability and mechanical behavior of additively manufactured functionally graded porous metallic biomaterials. *Acta Biomater.* 84, 437–452. doi: 10.1016/j.actbio.2018.12.013

Zhao, D., Witte, F., Lu, F., Wang, J., Li, J., and Qin, L. (2017). Current status on clinical applications of magnesium-based orthopaedic implants: A review from clinical translational perspective. *Biomaterials* 112, 287–302. doi: 10.1016/j.biomaterials.2016.10.017

Zhao, S., Li, S. J., Wang, S., Tao, H., Li, Y., Zhang, L., et al. (2018). Compressive and fatigue behavior of functionally graded Ti-6Al-4V meshes fabricated by electron beam melting. *Acta Mater.* 150, 1–15. doi: 10.1016/j.actamat.2018.02.060

Zheng, Y. F., Gu, X. N., and Witte, F. (2014). Biodegradable metals. *Mater. Sci. Eng. R Rep.* 77, 1–34.

Zhou, Y., Wu, P., Yang, Y., Gao, D., Feng, P., Gao, C., et al. (2016). The microstructure, mechanical properties and degradation behavior of laser-melted MgSn alloys. *J. Alloys Compd.* 687, 109–114. doi: 10.1016/j.jallcom.2016.06.068

Zumdick, N. A., Jauer, L., Kersting, L. C., Kutz, T. N., Schleifenbaum, J. H., and Zander, D. (2019). Additive manufactured WE43 magnesium: a comparative study of the microstructure and mechanical properties with those of powder extruded and as-cast WE43. *Mater. Charact.* 147, 384–397. doi: 10.1016/j.matchar.2018.11.011

Conflict of Interest: The authors declare that the research was conducted in the absence of any commercial or financial relationships that could be construed as a potential conflict of interest.